Arteannuin-B and its Spiro-isoxazoline Derivative Inhibits LPS Induced Pro-Inflammatory Responses in RAW 264.7 Macrophages and BALB/c Mice via down-regulation of NF-κβ/P38 MAPK Mediated Stress Signalling

Gifty Sawhney
CSIR-Indian Institute of Integrative Medicine
Javeed Ur Rasool
CSIR-Indian Institute of Integrative Medicine
Diksha Saroch
CSIR-Indian Institute of Integrative Medicine
Mumin Ozturk
University of Cape Town
Suraj Parihar
University of Cape Town
Frank Brombacher
University of Cape Town
Bilal Ahmad
Ajou University
Asha Bhagat
CSIR-Indian Institute of Integrative Medicine
Asif Ali
CSIR-Indian Institute of Integrative Medicine
Zabeer Ahmed (zahmed@iiim.res.in)
CSIR-Indian Institute of Integrative Medicine

Research Article

Keywords: Inflammation, Tumor necrosis factor-alpha (TNF-α), Interleukin-6 (IL-6), Nitric oxide (NO), RAW 264.7 cells, Lipopolysaccharide (LPS)

Posted Date: July 29th, 2022

DOI: https://doi.org/10.21203/rs.3.rs-1881315/v1

Arteannuin-B and its Spiro-isoxazoline Derivative Inhibits LPS Induced Pro-Inflammatory Responses in RAW 264.7 Macrophages and BALB/c Mice via down-regulation of NF-κβ/P38 MAPK Mediated Stress Signalling

Gifty Sawhney [a, c], Javeed Ur Rasool [b, c], Diksha Saroch [a], Mumin Ozturk[e], Suraj Parihar [e,f], Frank Brombacher [e,f], Bilal Ahmad [g], Asha Bhagat [a], Asif Ali [b, d] and Zabeer Ahmed [a,c *]

[a] Pharmacology Division, CSIR-Indian Institute of Integrative Medicine, Canal Road, Jammu-Tawi, J&K 180001, India.
[b] Natural Product and Medicinal Chemistry Division, CSIR-Indian Institute of Integrative Medicine, Canal Road, Jammu-180001, India.
[c] Academy of Scientific and Innovative Research (AcSIR), Ghaziabad-201002, India.
[d] CSIR-Institute of Genomics and Integrative Biology, Sukhdev Vihar, New Delhi, Delhi 110025, India.
[e] International Centre for Genetic Engineering and Biotechnology (ICGEB), Cape Town, South Africa.
[f] Wellcome Centre for Infectious Diseases Research in Africa (CIDRI-Africa), Division of Medical Microbiology, and Institute of Infectious Diseases and Molecular Medicine (IDM), Department of Pathology, Faculty of Health Sciences, University of Cape Town, Cape Town, South Africa.
[g] Department of Molecular Science and Technology, Ajou University, Suwon 16499, Korea

* Corresponding author email: zahmed@res.iiim.in

Abstract

Amongst the most significant scientific findings in the last two decades has been the role of inflammatory processes in protecting the host against the causative agents of injury. In this work, we examined the anti-inflammatory activities of Arteannuin-B **(1)** and its novel spirocyclic-2-isoxazoline derivative (**2**). Various anti-inflammatory assays were performed in lipopolysaccharide (LPS) induced RAW 264.7 macrophages using enzyme-linked immunosorbent assay, flow cytometric analysis, and western blotting. As a result, treatment with **(2)** decreased LPS-stimulated inducible nitric oxide synthase protein expression (iNOS), as well as production of nitric oxide (NO), tumor necrosis factor-alpha (TNF-α), and interleukin-6 (IL-6) in LPS induced RAW 264.7 cells. Additionally, the effects of (**1**) and **(2)** in an acute inflammatory condition were investigated *in-vivo* by using models like carrageenan-induced paw edema assay, acetic acid-induced writhing and tail immersion model in experimental mice, suggesting that **(2)** is a more potent anti-inflammatory candidate as compared to (**1**) with very low cell toxicity. In addition, biocomputational studies and histopathological analysis were also performed to validate the efficiency of **(2)** as compared to **(1)**.

Keywords: Inflammation, Tumor necrosis factor-alpha (TNF-α), Interleukin-6 (IL-6), Nitric oxide (NO), RAW 264.7 cells, Lipopolysaccharide (LPS), **(1)**.

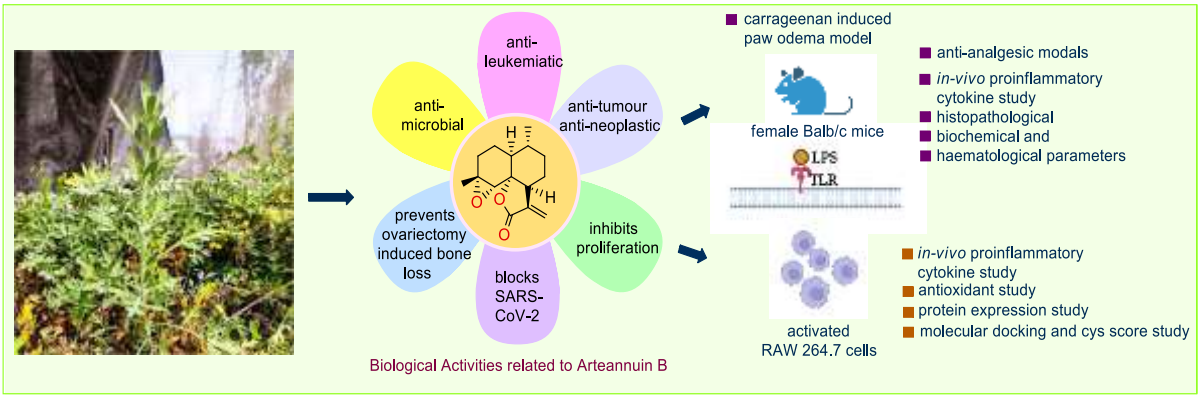

Graphical abstract showing different biological activities exhibited by **(1)**.

1. Introduction:

Inflammation is characterised by the activation of immune and non-immune cells that guard the host organism against viral and bacterial invasion to promote tissue repair and regeneration. However, chronic inflammation may arise if these processes go unchecked [1-5]. Inflammatory processes and immune system defines a broad range of physical and mental health issues that control morbidity and mortality due to ischemic heart disease, diabetes, renal infections, non-alcoholic fatty liver disease (NAFLD), and neurodegenerative disorders. Therefore, urgent need of innovative anti-inflammatory medication exists due to the resistance and side effects of the current drugs in use.

The immune system cells initiate various kinds of inflammatory defensive reactions and when activated, these immune cells augment the synthesis of several pro-inflammatory proteins/enzymes, including pro-inflammatory cytokines, such as interleukins IL-6 and tumor necrosis factor-α (TNF-α) and the production of inducible nitric oxide synthase (iNOS). These pro-inflammatory biomarkers are the most known mediators of inflammatory mechanisms [6, 7]. Due to the activation of the transcription factor by a number of mediators and cytokines, NF-kB has attracted attention for inflammatory-mediated responses [8-10]. Toll-like receptors (TLRs), which are expressed on macrophages cause pathogenic bacteria to induce NF-kB upon stimulation [11]. IkB (inhibitors of NF-kB) proteins prevent these transcription factors from becoming active in the cytoplasm of inactive cells. IkB kinase controls the activation of NF-kB [12-14]. IkB is phosphorylated by IKK, which causes NF-kB to become active. The pro-inflammatory and anti-inflammatory enzymes and cytokines' activities delicately balance the immune system's operation [15]. However, NF-kB must control the production of inflammatory mediators like inducible nitric oxide synthase (iNOS), tumour necrosis factor-α (TNF-α), and interleukin-6 (IL-6), as these substances not only aid in the elimination of encroaching pathogens but can also, if produced in excess, cause harmful inflammatory reactions like those seen in chronic inflammatory diseases (e.g., rheumatoid arthritis and septic shock) [16].

Phosphorylation of mitogen-activated protein kinases (MAPKs) like p38-MAPK, extracellular signal-regulated kinase (ERK) is a crucial step for the production of pro-inflammatory cytokines in activated macrophages [12]. Therefore, significant investigations have been performed in order to find out the safe and potent anti-inflammatory candidates

that could involve the expression of inflammatory proteins via upstream signalling mechanisms.

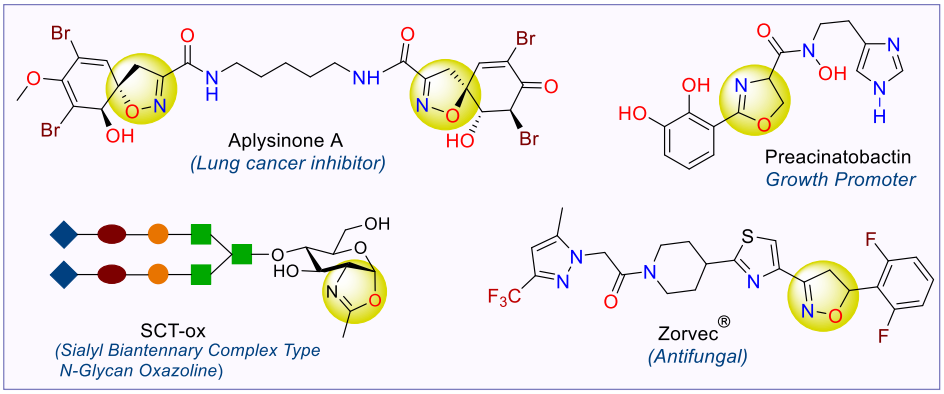

Figure 1: Some isoxazoline based scaffolds products used as drugs

On the other hand, heterocyclic scaffolds like substituted spirocyclic-2-isoxazolines are the structural building block of many biologically active scaffolds (Figure 1) and molecular leads in inflammation drug discovery [17-21]. The therapeutic efficacy of **(1)** has been investigated in recent years for its anti-neoplastic action *in-vitro* [22, 23], apoptosis [23, 24], anti-leukemia [24, 25], and anti-proliferative activity in breast cancer cells, lung, cervical, and liver [25]. Previously, we have reported the synthesis and anti-inflammatory screening of spiro-isoxazoline stitched adducts of (**1**) which furnished (3-chlorophenyl)-2-spiroisoxazoline arteannuin B (**2**) as a potent compound with lower toxicity. In continuation of the previous study, here in, we further investigated and validated the *in-vitro* and *in-vivo* efficacy of **(1)** for the attenuation of its inflammatory response as part of the programme for the biological potential of beneficial phytochemicals. Therefore, the present work highlights the investigation of inhibitory efficacy of **(1)** and **(2)** on the transcription of iNOS, TNF-α, and IL-6 in LPS-induced RAW 264.7 murine macrophage cells with the aim to explore the underlying biological pathway involved in inflammatory mechanism.

2. Materials and Methods:

2.1. Collection of plant material, extraction, isolation, and characterization:

Air-dried leaves of Artemisia *Annua* (5.0 kg) were collected from the CSIR-Indian Institute of Integrative Medicine's Botanical Garden at Srinagar, India. The air-dried leaves were extracted with DCM:MeOH (1:1) and evaporated under reduced pressure (360g). After fractionation with EtOAc: Hexane (1:9), the crude extract was subjected to chromatography over silica gel. White crystals of **(1)** were obtained (4.5g) [26].

2.1.2. Structure of Artennuin-B (1) and (3-chlorophenyl)-2-spiroisoxazoline Arteannuin B (2):

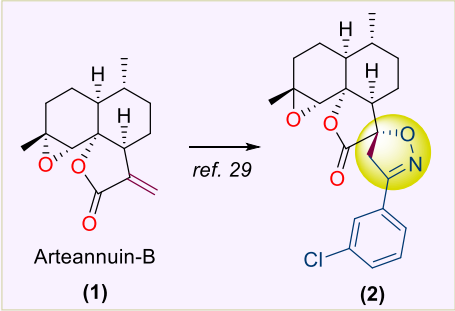

Figure 2: Structure of Arteannuin-B and (3-chlorophenyl)-2-spiroisoxazoline.

3. Evaluation of anti-inflammatory activity:

3.1. Preliminary Experiments:

3.1.1. Materials and Chemicals

Streptomycin (100ng/mL) and penicillin (100U/mL) were purchased from Sigma; 96 well plates were provided by NUNC, Germany, while GIBCO provided fetal bovine serum (FBS). DMSO, dexamethasone, lipopolysaccharides (LPS - Escherichia coli O111:B4), -nitro-L-arginine methyl ester (L-NAME), Griess reagent (1% sulfanilamide/0.1% naphthyl ethylenediamine dihydrochloride in 2.5% H_3PO_4), camptothecin, 3-(4,5-dimethylthiazol-2-yl)-2,5-diphenyltetrazolium bromide (MTT) were bought from Sigma, IL-6 and TNF-α ELISA Kits were procured from Invitrogen. Synergy Mx microplate reader belonged to Biotek, USA. P-IκB, T-IκB, P-p65-NF-κB, T-p65-NF-κB, P-p38-MAPK, and T-p38 MAPK, GAPDH, and anti-rabbit IgG horseradish peroxidase (HRP) conjugated secondary antibodies were purchased from Cell Signaling Technology (Danvers, MA).

3.1.2. Cell culture

RAW 264.7 macrophages were procured from ATCC, Rockville, MD, USA, were grown in GIBCO's Dulbecco's Modified Eagle Medium (DMEM) supplemented with 10% fetal bovine serum (FBS), 100U/mL penicillin, and 100ng/mL streptomycin, and incubated at 37°C in a 5% CO_2 environment. Cells were used between the third and fourth passages for all the experiments described as under.

3.1.3. Cell viability assay by MTT assay

RAW 264.7 macrophages were seeded and grown into 96 well plates (20,000 cells per well) for 24h. The cells were treated with test molecules- **(1)** and **(2)** for 48 hours, camptothecin (positive control), or vehicle control (0.1% DMSO) before being combined with 20µL of MTT solution (final concentration of 0.25mg/mL). After 4 h of incubation, the supernatant was removed, the formazan crystals were dissolved in 100µL DMSO, and absorbance at 570 nm was measured with a Synergy Mx microplate reader (Bio-Tek, USA). The cells' survival was determined using the formula below. The average of quadruplicate determinations with the mean standard error was used to illustrate the findings (SEM).

$$\%\text{cell viability} = \frac{(\text{absorbance of treated cells})}{(\text{absorbance of untreated cells})} \times 100$$

3.1.4. Measurement of Nitrite by Griess reaction

RAW 264.7 macrophages were seeded at a density of 1×10^5 cells per well in 96-well plates. After 24 hrs of incubation, these cells were treated with 1µg/mL LPS and different concentrations of test drugs. The nitrite (NO^-_2) level in the culture medium was used to evaluate the effectiveness of NO release. This was performed by mixing an equal ratio of the supernatant with the Griess reagent (1:1). After 10 min of incubation at room temperature, optical density was determined at 540 nm. The concentration of nitrite was determined using a $NaNO_2$ standard curve. The NO % inhibition was computed using the equation below, with the LPS stimulated group's nitrate level serving as the control.

$$\text{NO inhibition } (\%) = \frac{[\text{NO2}]\text{control} - [\text{NO2}]\text{sample}}{[\text{NO2}]\text{control}} \times 100$$

3.1.5. Detection of cytokine production

RAW 264.7 cells were seeded at a density of 2×10^5 cells/well in 96-well plates. After an overnight incubation, the cells were treated with the test molecules and dexa (10µM) was used as a positive control. After one hour of treatment, 1µg/mL LPS was added and incubated for 24h. After 24 h, the cell culture supernatants were collected, and TNF-α and IL-6 levels were determined using ELISA Kits (Invitrogen) according to the manufacturer's instructions. A standard curve was used to quantify the concentrations of TNF-α and IL-6 in the samples. An equation was used to compute the percent inhibition, displayed below. The data is the average of three independent determinations with a standard mean error (SEM).

$$\%\text{inhibition} = \left[\frac{\text{C} - \text{D}}{\text{C}}\right] \times 100$$

where C=Vehicle control group data, D=Treated group data

3.2. Measurement of intracellular ROS by DCFH-DA staining

RAW 264.7 cells were plated in a six-well culture plate, at the concentration of 1×10^6 cells per well and treated with 1µg/mL LPS for 24 h and different concentrations of **(1)** and **(2)**. The cells were washed twice in 1xPBS to eliminate the extra nanoparticles. After 30 minutes of incubation with 10mM DCFH-DA at 37°C, the cells were washed twice with 1xPBS. The DCFH-DA fluorescent probe was used to measure intracellular ROS. DCFH-DA may be oxidized to the highly fluorescent chemical dichlorofluorescein by intracellular H_2O_2 or low-molecular-weight peroxides (DCF). Flow cytometry and a fluorescent microscope (Nikon Corporation, Chiyoda-ku, Tokyo, Japan) were used to investigate ROS generation in the cells (BD FACS Aria III, 488 nm excitation, 530-540 nm emission). A minimum of 20,000 events were examined in each sample, with the results presented as a fold-change in fluorescence intensity over time.

3.3. Molecular docking and Cyscore analysis.

(1) and **(2)** were docked on NF-κB (Protein databank **(PDB) ID: 3GUT**) by employing the Molecular Operating Environment (MOE) 2019.01 docking program. The NF-κB PDB structure was retrieved from the RCBS protein database. The breaks in the structure were repaired. The partial charges were added to the proteins after water molecules were removed and hydrogen atoms were added. MOE2019.01 was used to reduce the protein architectures utilizing the Optimized potential for liquid simulations (OPLS) force field. In ChemDraw, the 3-dimensional structure of **(2)** and **(1)** was created, and the MMFF94x force field was used to reduce the structure in **MOE2019.01**. After protein and ligand preparation, the ligands **(2)** and **(1)** were docked on NF-κB at the dimeric interface and DNA binding sites. The docked solutions were clustered based on root mean square deviation and docking score. Representative members of the populated cluster were analyzed for binding affinity by cys-score analysis [27]. In addition, we evaluated the ADME properties of **(2)** and **(1)** by utilizing SwissADME [28]**.**

3.4. Cell lysate preparation and Western blot analysis

RAW 264.7 macrophage cells (2 x 10^5cells/well) were plated on a 6-well plate and treated for 24 h with or without **(1)** and **(2)** (5-10μM) and LPS at the concentration of 1μg/mL was added after 45 minutes of drug treatment. After incubation, the supernatant was removed, and the cells were rinsed in ice-cold 1X PBS (1ml, pH 7.4). RIPA buffer was prepared with 50 mM NaF, 0.5 mM Na-Orthovanadate, 2mM PMSF, phosphatase, and on the ice at 4˚C, protease inhibitor cocktail for 30 minutes. The sample was transferred to each sterile tube, and the samples were spun at 13000rpm for 15 minutes. The cell debris was removed, and the supernatant was transferred to other sterile tubes. The sample was further concentrated using Speed Vac until all the solution evaporated or less than 50μl remained. The samples were again re-suspended in 100μl ice-cold 1X PBS. Thermo Scientific PierceTM BCA Protein Assay Kit was used to quantify the protein concentration. 10% SDS-polyacrylamide gel was used to separate 25μg of proteins, which were then transferred to nitrocellulose (NC) membranes. All NC membranes were blocked using 2% BSA in TBST (150mM NaCl, 19mM Tris-HCL, 0.1% Tween-20 (TBS-T) buffer on a shaker for 2 hrs. The membranes were incubated overnight with primary antibodies to identify the target proteins specific for IκB, NF-κB P65, p38 MAPK and GAPDH at 4˚C. After three 5-minute washes with TBS-T solution, the membrane was incubated for 1 h at room temperature with HRP-linked anti-mouse, anti-rabbit, or anti-goat immunoglobulin G secondary antibodies. The membrane was rewashed with acquiring kit wash buffer (SERA CARE kept at 4˚C) three times for 5 minutes each. The detection method used was enhanced chemiluminescence (ECL), ChemiDOC (Davinch-K, Davinch-Invivotm) imaging system to obtain the pictures.

3.5. In-vivo anti-inflammatory activity

3.5.1. Animals

BALB/c mice (female, 6–8 weeks old, 20-25 g) were kept under standard laboratory conditions: 23 ± 1°C, 55 ± 10% relative humidity, 12/12 h light/dark cycles, and free access to water and standard pellet food (Lipton India Ltd.). All animal studies followed the

guidelines laid out in the Guide for the Care and Use of Laboratory Animals (National Research Council 2011). The Institutional Animal Ethics Committee authorized all of the protocols employed in the experiment.

3.5.2. Acute toxicity studies

(1) and **(2)** were tested for acute toxicity in healthy female BALB/c mice. The mice were placed into six groups, each with five female BALB/c mice (one control group and five treatment groups). Mice were administered with dosages of 100, 200, 300, 400, and 500 mg/kg body weight as a single oral gavage. Only the same amount of 0.9% normal saline water was given to the control group. The mice's general behaviour, indications of toxicity, and death were closely monitored for 120 minutes and then once daily for the next 14 days following the treatment. Even animals that died beyond the first observation period had their data utilized in the final evaluation of the test outcome. After 14 days, the number of survivors was recorded.

3.5.3. *In-vivo* LPS challenge and serum cytokine detection.

LPS (1 mg/kg; Sigma) was given intraperitoneally to female BALB/c mice (6–8 weeks old) with or without **(1)** and **(2)**. The LPS were prepared in ice-cold, sterile phosphate-buffered saline before use (PBS). The negative and positive controls were PBS or Dexa (10 mg/kg), corresponding to the clinical dosage. Mice were euthanized 2 h after injection, and the blood samples were collected in BD Vacutainer SST tubes from the retro-orbital plexus of mice for harvesting serum. Blood tubes were left to coagulate at ambient temperature for 15-30 minutes after collection. The samples were subjected to centrifuge at 1,500 x g for 10 minutes. The top layer of serum was carefully transferred into a fresh 1.5 mL Eppendorf tube and refrigerated at -20 C until analysis.

3.6. Analgesic activity of (1) and (2)

Analgesic activity of **(1)** and **(2)** was evaluated using the acetic acid-induced writhing test and tail immersion test in mice.

3.6.1. Acetic acid writhing test.

The procedure was demonstrated by Koster et al. in 1959. In essence, mice were given a standard analgesic drug, diclofenac sodium (20 mg/kg, i.p.), **(1)** and **(2)** (40, 20, 10, 5, 1mg/kg orally), 30 minutes before intraperitoneal injection of 0.6 % glacial acetic acid (10 ml/kg body weight). For each group of mice, the number of writhes (a wave of abdominal muscle contractions followed by hind-limb extension is the hallmark of this condition) was counted from 5 minutes after acetic acid administration to 20 minutes after injection and represented as a percentage of protection. Analgesic properties were evidenced by a decrease in the number of writhes. The following formula was used to compute the percentage of protection against the writhing caused by acetic acid:

$$\% \text{ Protection} = \frac{\text{Nc} - \text{Nt}}{\text{Nc}} \times 100$$

where Nc is the number of writhing in control, and Nt is the number of writhing in test animals.

3.6.2. Tail immersion test.

The tail immersion test was used to assess the analgesic activity of **(1)** and **(2)**, as explained by Aydin. Thirty minutes before and after intraperitoneal administration of the standard analgesic drug, diclofenac sodium (20 mg/kg, i.p.), and subcutaneous injection of **(1)** and **(2)**, the response time was assessed after that every 30 minutes up to 120 minutes.

3.7. Carrageenan-induced rat paw edema test

Carrageenan-induced paw edema in mice is a well-established model of acute inflammation for testing anti-inflammatory medicines. As previously disclosed, the anti-inflammatory activity of **(1)** and **(2)** was examined in mice with carrageenan-induced paw edema. Carrageenan (0.1 ml of 1% w/v solution) was injected under the plantar aponeurosis in the right hind paw of rats to cause acute inflammation. The inflammation was quantitated by using a digital plethysmometer in milliliters (mL), i.e., edema causing water displacement, before and after Carrageenan injection at +1, +3, +6, +8, and +10 h. The percent inhibition of edema was analyzed quantitatively using a vehicle-treated control group. The percentage inhibition of edema was calculated using a vehicle-treated control group for each group. The difference between the volume at 0 h and the volume at +1 h indicates paw edema in the first hour after carrageenan administration. As a result, paw edema was determined at 0, 1, 3, 8, and 10 hours. After that, the percentage of paw edema inhibition was calculated using the formula:

$$\%\text{inhibition of paw edema} = \frac{\text{Vc} - \text{Vt}}{\text{Vt}} \times 100$$

3.8. Clinical Pathology

The blood samples were obtained from the eye and collected in a tube coated with 10 % heparin for haematology and from the heart for clinical chemistry testing after the treatment period. Total white blood cell (WBC), Red blood cell count (RBC), hematocrit (HCT), mean corpuscular volume (MCV), platelet count (PLT), and differential leukocyte count were among the haematological parameters examined. Serum alkaline phosphatase (ALP), alanine aminotransferase (ALT), Total bilirubin, blood creatinine, Glucose, and serum aspartate aminotransferase (AST) were also measured.

3.9. Tissue collection and histopathological examination

All of the animals were euthanized after the experiment. The kidneys, liver, lungs, and paw were collected and moistened immediately after dissection to minimize drying. Animal organs and the tissues were stored in 10% neutral buffered formalin for at least 48 h prior to trimming and processing for histopathological examination in both the control and test groups. The tissues were fixed and embedded in paraffin, sectioned to 4 to 5μm thickness using a microtome, mounted on glass microscope slides, stained with eosin and hematoxylin, and viewed under light microscopy.

Results

4.1. (1) and (2) did not alter the cell viability confirmed by the MTT assay

As depicted in Figure 3, **(1)** and **(2)** did not alter cell viability of RAW 264.7 after a 48 h treatment, with concentrations ranging from 1µM to 10µM. However, the highest dose (10µM) of **(1)** tested resulted in 86.9% cell viability, whereas the highest dose (10µM) of **(2)** resulted in 89.05% cell viability. As a result, the pharmacological effects of the **(1)** and **(2)** drugs were evaluated at lower, non-cytotoxic dosages in 48 h experiments. Our data revealed that (1-10µM), **(1)** and **(2)** are non-toxic, and thus they may be used to explore the anti-inflammatory effect on RAW 264.7 cell line.

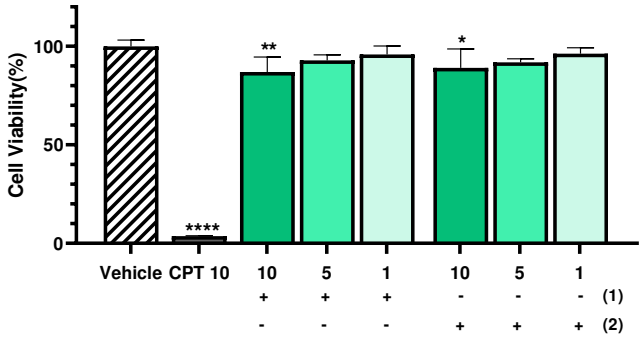

Figure 3. The effect of **(1)** and **(2)** on % cell viability in RAW 264.7 cells. The cells were treated with different concentrations of **(1)** and **(2)**, and the cell viability was determined by MTT assay after 48 h treatment. The results shown are the mean ± standard deviation of three independent experiments. Statistical significance was assessed by one-way ANOVA followed by Dunnett's test, ****$p < 0.0001$; **$p<0.005$, *$p<0.05$ vs vehicle alone. All the values were mean ± SD, n=4. CPT: Camptothecin

4.2. Effect of (1) and (2) on the production of inflammatory mediator-Nitric oxide in LPS-induced RAW 264.7 cells.

Our study demonstrated that compared to L-NG-Nitro arginine methyl ester (L-NAME), a known NO inhibitor, **(1)** and **(2)** suppressed LPS-stimulated nitrite levels in a dose-dependent manner (Figure 4). L-NAME and Dexa were used as positive controls, and they suppressed the levels of nitric oxide from 80.38µM to 45.61µM and 44.5µM, respectively. **(1)** has suppressed the release of nitric oxide to 23.29µM at 10µM, 36.26 at 5µM, 48.65 at 1µM whereas **(2)** has suppressed to 16.43µM at 10µM, 31.62 at 5µM, 40.97 at 1µM proving to be a better nitric oxide inhibitor as compared to its parent compound, Arteannuin-B.

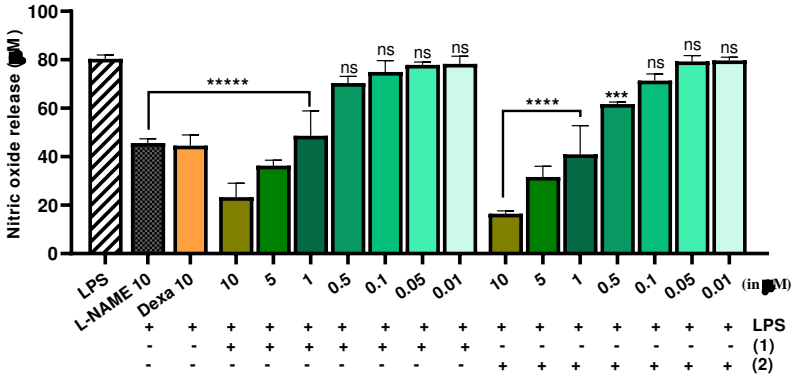

Figure 4: Comparative effect of **(1)** and **(2)** on nitric oxide release in LPS stimulated RAW 264.7 cells. The cells were treated with different concentrations of **(1)** and **(2)** for 1h, and LPS (1µg/ml) was then added for 24h. The levels of nitric oxide in the cell culture supernatant were measured by using the Griess reagent assay. Statistical significance was assessed by one-way ANOVA followed by Dunnett's test, ****p < 0.0001; ***p < 0.005 vs LPS alone. The results shown were mean ± standard deviation of three independent experiments. All the values were mean ± SD, n=3. Dexa: Dexamethasone; LPS: lipopolysaccharides; L-NAME: L-NG-Nitro arginine methyl ester.

4.3. Effect of (1) and (2) on the production of TNF-α and IL-6 in LPS-induced RAW 264.7 cells.

As indicated in Figure 5A, at a concentration of 10 µM, **(1)** and **(2)**, effectively inhibited LPS-induced release of TNF-α (72.18%), IL-6 (68.43%) and TNF-α (81.58%), IL-6 (83.34%) as compared with those of the control- Dexa which showed percentage inhibition of TNF-α (61.18%), IL-6 (54.56%), respectively. Additionally, in the case of IL-6 (Figure 5B), **(2)** even at 5 µM, has exhibited the high percentage inhibition of 55.9% as compared with 48.5% **(1)** at 5µM and 54.5% Dexa (10µM). These results indicate that **(2)** inhibited LPS-induced pro-inflammatory cytokines production efficiency compared to **(1)** in RAW 264.7 macrophages.

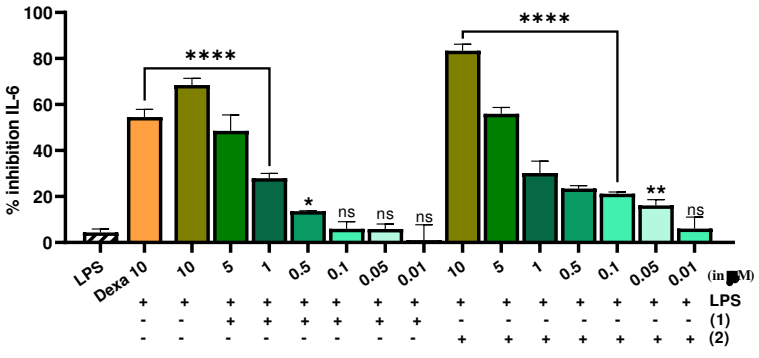

5A.

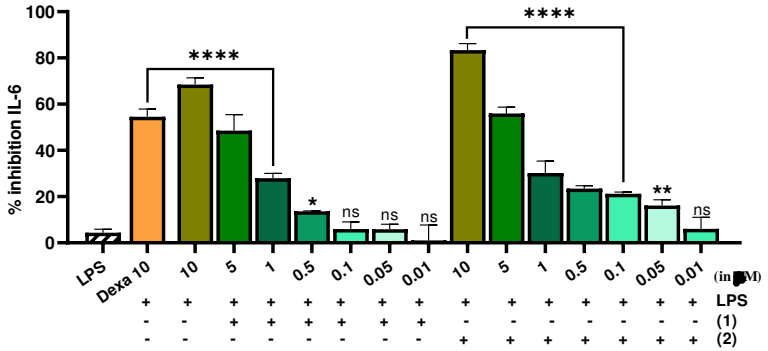

5B.

Figure 5A and 5B: Comparative effect of **(1)** and **(2)** on TNF-α and IL-6 release in LPS stimulated RAW 264.7 cells. The cells were treated with different concentrations of **(1)** and **(2)** for 1h, and LPS (1µg/ml) was then added for 24h. The levels of TNF-α and IL-6 in the cell culture supernatant were measured using ELISA. All values were mean ± SD, n=3. (****P<0.0001, **P<0.005. *P<0.05) indicated a significant difference with the LPS treated cells assessed by one-way ANOVA followed by Dunnett's test. LPS: lipopolysaccharide; Dexa: Dexamethasone; TNF-α: tumor necrosis factor-alpha; IL-6: interleukin-6.

4.4. Relative effects of (1) and (2) in inhibiting the production of reactive oxygen species by fluorescence microscopy and flow cytometry

Because activated macrophages produce a substantial quantity of reactive oxygen species (ROS) during inflammation, we measured intracellular ROS in LPS-stimulated RAW 264.7 macrophage cells, which showed a 95.75% increase in ROS compared to untreated cells. At 10µM, pretreatment of **(2)** compared to **(1)** significantly reduced ROS generation to 35.69% and 40.23%, respectively, in LPS exposed RAW 264.7 cells (Figure 6).

6.

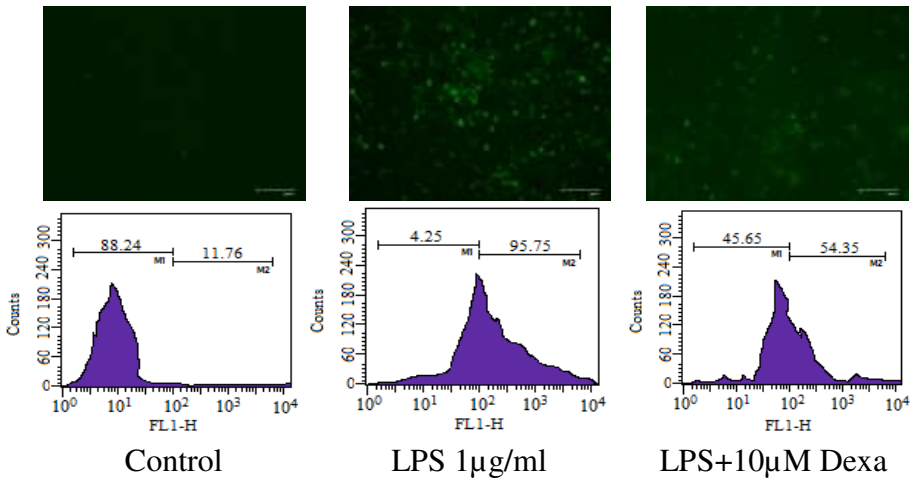

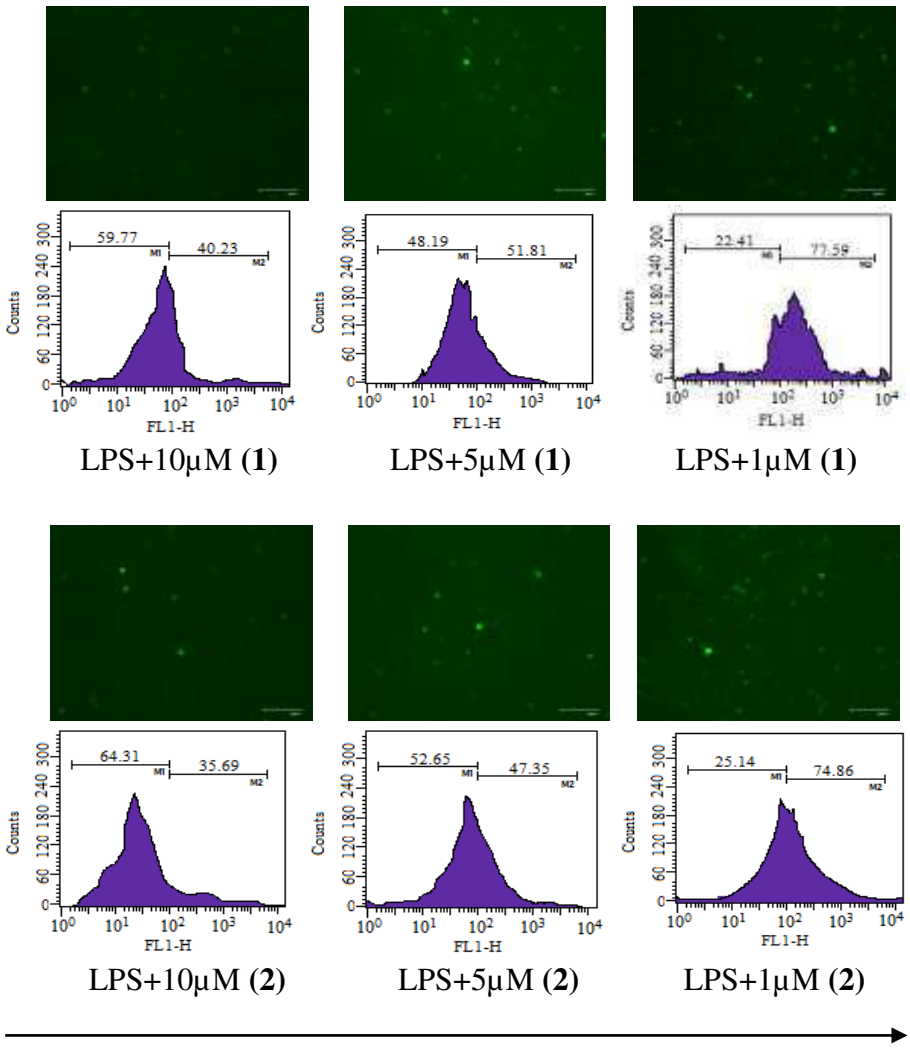

Figure 6: Effect of **(1)** and **(2)** on LPS-induced release of ROS: To determine the effect of **(1)** and **(2)** on the intracellular ROS production, treated RAW 264.7 cells were incubated with DCFH-DA (10mM) for 30mins. The relative fluorescence intensity of fluorophore DCFH-DA was then measured and detected using BD FACS Aria III flow cytometer (488 nm excitation, 530-540 nm emission), respectively. The results shown are the mean ± standard deviation of three independent experiments.

4.5. Molecular docking and cys score analysis

To assess the behavior of **(1)** and **(2)** in the binding site of NF-κB, the molecular docking was performed by MOE2019. The dimeric interface site (Figure 7A) and DNA binding site (Figure 7B) were used as binding sites. At the dimeric interface, the **(2)** showed interaction with Glue211, Asp243, Arg253, Phe239, and Ser238 (Figure 7A, vi). **(1)** showed similar interactions at the dimeric interface site (Figure 7A, iii). Analyzing the interaction of the docked solution at the DNA binding site (Figure 7B), the **(2)** showed ionic interaction with Lys374 and arene type interaction with Tyr379 (Figure 7B, vi). In addition to these interactions, **(2)** engages with Arg351, Lys349, Lys377, His364, Gly366, Gly365, and Phe353 (Figure 7B, vi). Likewise, **(1)** interacts with Arg351, Phe353, Gly352, Lys349, and

Lys374 (Figure 7B, iii). **(1)** showed the ionic interaction with Lys349 of NF-κB. The docking results showed that both **(1)** and **(2)** have more vital interactions at the DNA binding site of NF-κB.

A. Ligands docked at Dimeric site:

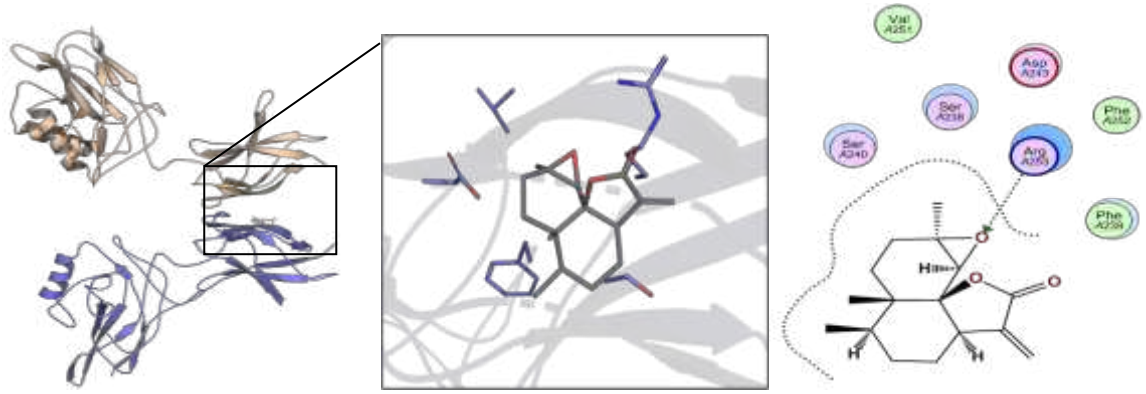

(1) **(i)** **(ii)** **(iii)**

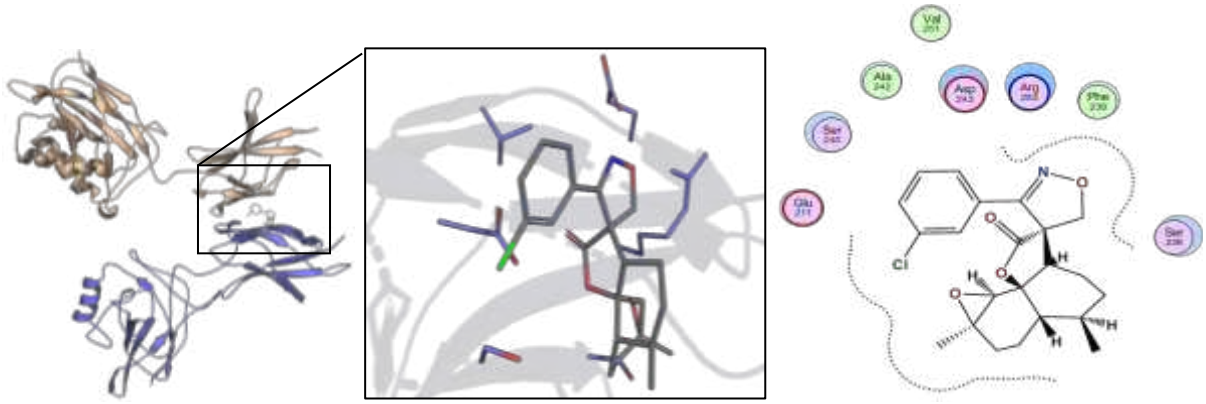

(2) **(iv)** **(v)** **(vi)**

B. Ligands docked at DNA-binding site:

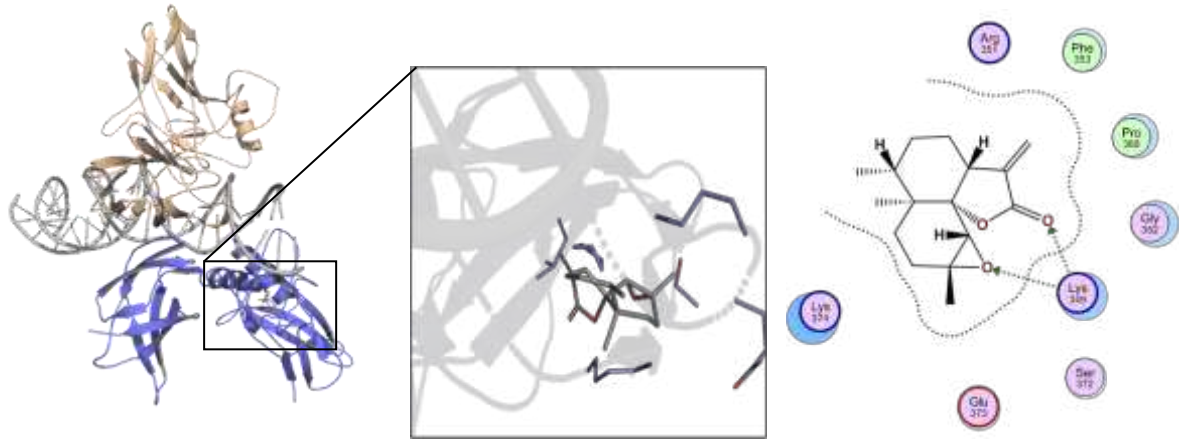

(1) **(i)** **(ii)** **(iii)**

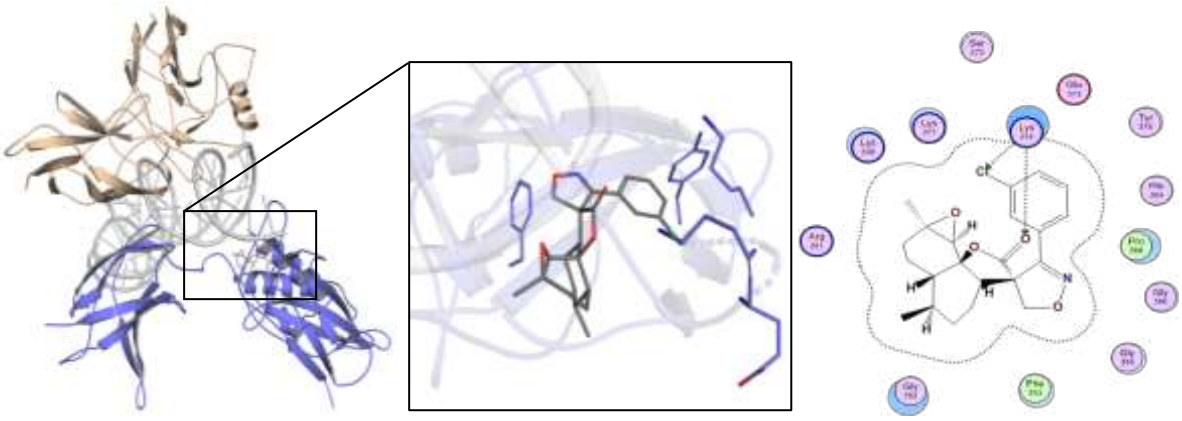

(2) **(iv)** **(v)** **(vi)**

Figure 7A and 7B: In-silico studies to determine the binding interaction of **(1)** and **(2)** with legends docked at dimeric interface site (7A) and DNA binding site (7B). The molecular operating environment (MOE2019) was used to assess the behaviour of **(1)** and **(2)** in the binding site of NF-κB. Green lines show the iconic interaction of the molecule with that of different amino acids.

The binding affinity of **(1)** and **(2)** was computed by cyscore analysis, as shown in Table 1. The docking score and binding affinity data showed that both molecules scored higher than the dimeric site. The docking and binding affinity data revealed that **(2)** and **(1)** have a higher affinity towards the DNA binding site of NF-κB. Further, we evaluate the ADME properties of these compounds by utilizing SwissADME. The ADME data (Table 1) showed that both molecules have the same pharmacokinetic and drug-likeness properties. **(2)** and **(1)** compounds were docked on NF-κB at the dimeric interface site and DNA interacting site. The docked solutions were clustered, and the most populated cluster was selected from which top representative members' docking score, cyscore score, and ADME properties are mentioned in Table 1.

Docking Site residues:

DNA binding Site residues: (GLY352 PHE353 ARG354 ARG356 GLY361 PRO362 SER363 HIS364 GLY365 GLY366 PRO368 GLY369 SER372 LYS374 LYS377 SER378 TYR379 VAL412 GLY413 ASN436 LEU437 GLY438 ILE439)

Dimeric Site Residues: (GLU211 SER238 PHE239 SER240 ASP243 VAL251 PHE252 ARG253)2:(ARG552).

Compound name	**Docking Score**		**Cyscore (Binding Affinity)**		**ADME**				
	Dimer-site	DNA site	Dimer-site	DNA site	Log $P_{o/w}$	Log S	Log K_p	TPSA	Bioavailability Score
(1)	-4.64	-4.80	-2.34	-2.53	3.89	-5.42	-5.61 cm/s	60.42 Å²	0.55

(2)	-4.65	-5.66	-2.54	-2.87	3.89	-5.42	-5.61 cm/s	60.42 Å²	0.55

Table 1 shows the binding affinity of **(1)** and **(2)** as computed by cyscore analysis, and the ADME properties were evaluated using SwissADME.

4.6. Effect of (1) and (2) on upstream signaling for NF-κB and MAPK activation in LPS-induced RAW 264.7 cells.

The regulation of inflammatory mediators in LPS-stimulated macrophages is transcriptionally linked with the NF-κB and MAPK pathways; therefore, we asked whether **(1)** and **(2)** have the potential to prevent the activation of these pathways. The effects of **(1)** and **(2)** on LPS-induced degradation and phosphorylation of inhibitory kappa B (IκB) protein were examined using immunoblotting. In a dose-dependent manner, **(1)** and **(2)** blocked LPS-induced phosphorylation of IκB in the cytosol (Figure 8A). When IκB-α and NF-κB are separated, free dimer-activated subunits of NF-κB (p50/p65) can be translocated from the cytosol to the nucleus. LPS alone increased the quantity of NF-κB in the nucleus, whereas **(1)** and **(2)** reduced LPS-induced nuclear translocation of NF-κB in a dose-dependent manner (Figure 8B). We determined the effect of **(1)** and **(2)** on LPS-stimulated phosphorylation of P-p38 and T-p38 MAPK in RAW 264.7 cells to see if suppression of NF-κB activation is mediated through MAPK pathways. LPS promoted phosphorylation of p38 significantly, as seen in Fig. 8B, 8C. LPS-stimulated phosphorylation of p38 MAPK was considerably reduced by pretreatment with **(1)** and **(2)**. This shows that **(1)** and **(2)** reduced the phosphorylation of p38. These findings suggest that, compared to MAPK, NF-κB may have a role in **(1)** and **(2)**'s ability to reduce NO and pro-inflammatory cytokines in activated macrophages.

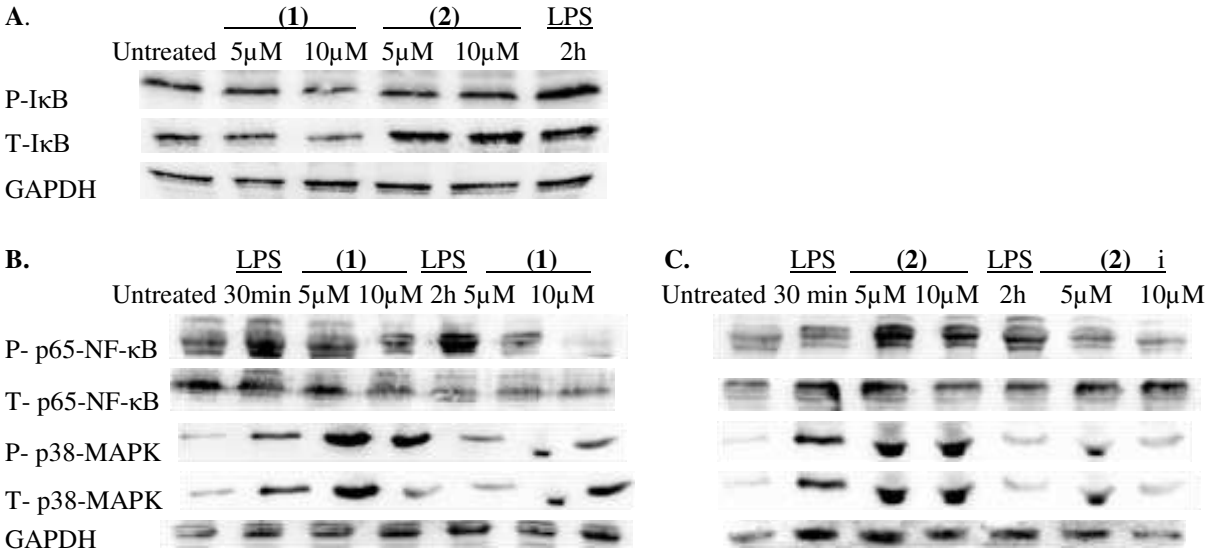

Figure 8A, 8B, 8C: Impact of **(1)** and **(2)** on the NF-κB and MAPK pathway in RAW 264.7 cells. (A, C, D) RAW 264.7 cells treated with **(1)** and **(2)** for 30 min and 2h were induced by LPS. The NF-κB and MAPKs signaling pathway expression proteins were detected using Western blotting.

4.7. Acute toxicity studies

The LD50 of **(1)** by intraperitoneal injection in mice, according to published research, is 1558 mg/kg [29]. We may usually pick a dosage between 1/5 and 1/50 of LD50. In the acute toxicity study, the oral LD50 of **(1)** and **(2)** was > 2000 mg/kg. As a result, according to a published study we chose 40 mg/kg for the current investigation [30]. Furthermore, no deaths, toxicity symptoms, or significant behavioural abnormalities were found, suggesting that **(1)** and **(2)** had a reasonable margin of safety. On day 14th, biochemical and haematological parameters were evaluated to determine any end-organ toxicity.

4.8. Effect of (1)and (2) on the production of TNF-α and IL-6 in the serum collected from LPS-induced BALB/c mice.

The acute peritonitis in mice design was induced following intraperitoneal injection of LPS (1mg/kg). **(1)** and **(2)** reduced LPS-induced production of pro-inflammatory cytokines, and chemokines in macrophages and DCs. As a result, we concentrated on **(1)** and **(2)**-mediated reduction of these cytokines' production *in-vivo*. This investigation used the glucocorticoid, Dexa- 10mg/kg as a positive control in LPS-challenged mice models because it is frequently used to treat sepsis or septic shock.
In serum cytokine assessment, we chose **(1)** and **(2)** dosages of 40 mg/kg, similar to doses of 10µM and 5µM in cellular assays *in-vitro*, respectively. When compared to the levels in animal models, **(1)** and **(2)** treated mice produced lower amounts of pro-inflammatory cytokines TNF-α and IL-6 in the sera, similar to the results *in-vitro* (Figure 9A and 9B).

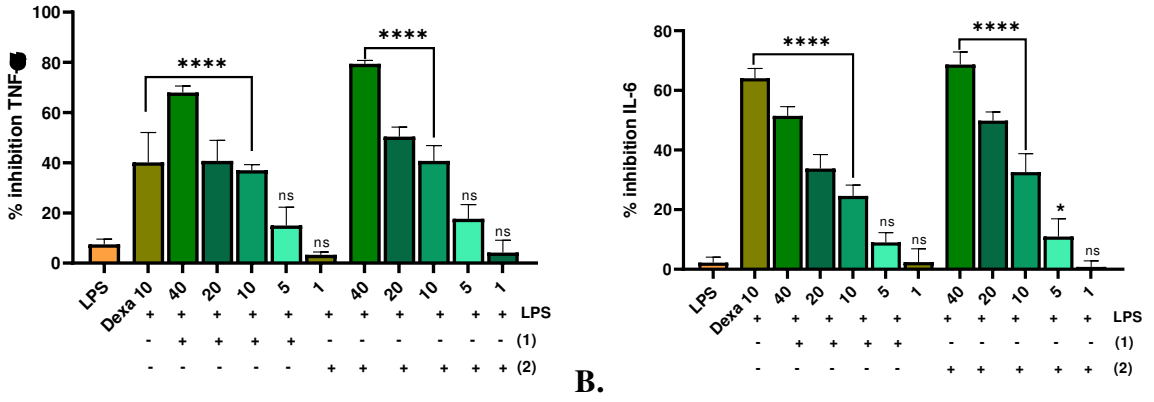

A. **B.**

Figure 9A and 9B: Comparative effect of **(1)** and **(2)** on pro-inflammatory cytokines TNF-α and IL-6 release in LPS (1mg/kg) stimulated female BALB/c mice 6-8 weeks old. **(1)** and **(2)** were drugged orally, blood was collected from R.O.P, and cytokine inhibition was measured in serum. The data represents the representative experiment's mean ± SD (n = 4). All values were mean ± SD, n=3. (****P<0.0001, *P<0.05 indicated significant difference with the LPS treated cells assessed by one-way ANOVA followed by Dunnett's test). LPS: lipopolysaccharide; Dexa: dexamethasone; TNF-α: tumor necrosis factor-alpha; IL-6: interleukin-6.

4.9. As compared to (1), (2) efficiently reduced the writhing caused by Acetic acid in the acetic acid-induced writhing syndrome model

In the writhing syndrome model, **(1)** and **(2)** showed a dose-dependent reduction in the number of writhes of test animals compared to the Diclofenac. **(1)** and **(2)**, at the doses of 40, 20, 10, 5 and 1 mg/kg p.o., reduced the writhing significantly in a dose-dependent manner by 53.03%, 43.74%, 23.97%, 10.94%, 7.48% and 60.21%, 53.29%, 33.05%, 23.01% and 8.25% respectively. Treatment with Diclofenac reduced writhing by 40.42% at a 20 mg/kg dose. The results of the writhing syndrome model are shown in Table 2 and Figure 10.

Group	Dose (mg/kg)	No. of Writhes	% Inhibition
Control	**0.2 ml/kg**	--	--
Diclofenac Sod. (ip)	**20**	15.09 ± 0.53	40.42 %
(1)	**40**	11.89 ± 0.68	53.03 %
	20	14.25 ± 1.91	43.74 %
	10	19.25 ± 0.31	23.97 %
	5	22.55 ± 1.58	10.94 %
	1	23.43 ± 0.16	7.487 %
(2)	**40**	10.07 ± 0.37	60.21 %
	20	11.83 ± 0.89	53.29 %
	10	16.95 ± 0.39	33.05 %
	5	19.5 ± 0.14	23.01 %
	1	23.24 ± 0.63	8.25 %

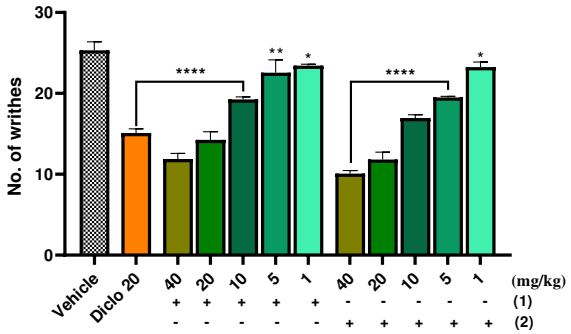

Table 2 and Figure 10: Table 2 shows the effects on writhing of **(1)** and **(2)** administered 30 min before intraperitoneal 0.6% acetic acid in mice. Each value represents mean ± S.E.M or percentage inhibition of pain as compared to control animals, n =5. Figure 10 shows percentage inhibition of **(1)** and **(2)** on writhing caused by 0.6 % acetic acid given to 6-8 week old female BALB/c mice. **(2)** showed a significant percentage inhibitory effect as compared to **(1)**. The data represents the representative experiment's mean ± SD (n = 4). All values were mean ± SD, n=3. (****P<0.0001, **P<0.001, *P<0.01 indicated significant difference with the LPS treated cells assessed by one-way ANOVA followed by Dunnett's test).

4.10. (2) efficiently increased the reaction time as compared to (1) in the tail immersion model

The tail immersion test investigated the effect of central-acting analgesic medications on increasing the reaction time of mice in response to hot water. As shown in Table 3, **(1)** and **(2)** had a strong analgesic effect from 30 minutes onwards, with the maximum effect occurring 120 minutes after treatment. The impact was statistically significant compared to the mice in the control group.

Group	Dose (mg/kg)	0 min	30 min	60 min	90 min	120 min
Control		2.59 ± 0.14	2.41 ± 0.11	2.53 ± 0.11	2.40 ± 0.04	2.37 ± 0.06
Diclofenac Sod.	**20**	2.43 ± 0.11	5.27 ± 0.21	6.49 ± 0.29	7.50 ± 0.20	7.84 ± 0.09
(1)	**40**	2.70 ± 0.14	3.43 ± 0.15	4.75 ± 0.24	5.45 ± 0.08	6.34 ± 0.21
	20	2.47 ± 0.09	3.16 ± 0.15	4.28 ± 0.8	4.89 ± 0.11	5.28 ± 0.36

	10	2.55 ± 0.18	3.07 ± 0.14	3.94 ± 1.32	4.45 ±0.06	4.67 ± 0.19
	5	2.61 ± 0.29	2.86 ± 0.05	3.55 ± 0.12	3.66 ± 0.29	4.15 ± 0.17
	1	2.49 ± 0.08	2.57 ± 0.09	2.85 ± 0.06	2.91 ± 0.04	3.69 ± 0.08
(2)	**40**	2.42 ± 0.12	5.21 ± 0.09	5.35 ± 0.21	5.70 ± 0.11	6.44 ± 0.39
	20	2.58 ± 0.14	4.5 ± 0.07	4.61 ± 0.30	5.2 ± 0.01	5.65 ± 0.02
	10	2.44 ± 0.10	4.42 ± 0.03	4.54 ± 0.01	5.08 ± 0.08	5.43 ± 0.16
	5	2.53 ± 0.30	4.19 ± 0.11	4.27 ± 0.11	4.34 ± 0.08	4.62 ± 0.32
	1	2.59 ± 0.16	3.44 ± 0.39	3.43 ± 0.39	3.84 ± 0.12	3.91 ± 0.04

Table 3 shows the effects of pre-treatment with **(1)** and **(2)** at intervals of 30 min on tail withdrawal in rats whose tails were dipped in hot water (55.0 ± 0.5 C). Each value represents mean ± S.E.M, n=5.

4.11. As compared to (1), (2) efficiently decreased the paw edema induced by carrageenan in the carrageenan-induced paw edema model

Subcutaneous injection of carrageenan elicited edema in mice, increasing in paw size, indicating acute paw inflammation. Figure 11A shows the inhibitory effect of **(1)** and **(2)** with 44.4% and 56% inhibition, respectively, in comparison to Dexa (20mg/kg) with 43.15% at 8th hr ($P \leq 0.01$). Photographs show the paws of mice in several groups, including normal control mice and carrageenan-induced paw edema animals given a placebo; dexa, **(1)**, and **(2)** have been shown in Figure 11A. These images showed a significant reduction in paw thickness in **(1)** and **(2)** treated groups compared to the control group.

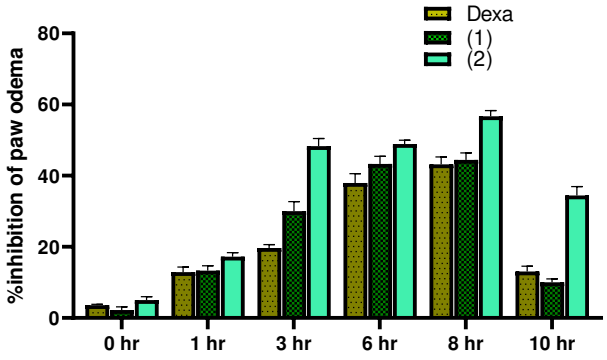

A.

B.

Figure 11A: Graphs showing an increase in the inhibitory effect of **(2)** compared to **(1)** and Dexa; the maximum effect was noticed at the 8th hr of the subcutaneous injection of carrageenan. Fig 11B: Plethysmometer is used for measuring paw edema.

Initial paw thickness or edema at 0th hr

Normal saline **Carrageenan** **Dexa** **(1)** **(2)**

Paw volume after 10th hr

Normal saline **Carrageenan** **Dexa** **(1)** **(2)**

Figure 11C: Comparative effect of **(1)** and **(2)** at 40 mg/kg dose on carrageenan-induced paw edema: Compounds or vehicle was administrated 1h prior to carrageenan injection (1%), and paw volume measured (a) mice were evaluated for percentage inhibition of paw edema at 10h post carrageenan injection.

4.12. Biochemical and haematological analysis done after the treatment of (1) and (2)

The serum biochemical analysis revealed no consistent changes between the treatment and control groups for BALB/c female mice (Table 4). Throughout the study, most means and individual concentrations in treated and control animals were within the reference range. At any moment, there were no statistically significant changes between the treatment and control groups in RBC, HCT, or MCV. Mean WBC counts in all groups were within the reference range throughout the trial. At no point did the mean RBC count differ between groups. There were occasional alterations in the treatment and control groups in neutrophil, lymphocyte, and monocyte counts.

S. No.	Parameters	Control	(1)		(2)		Reference ranges
			1mg/kg	40mg/kg	1mg/kg	40mg/kg	
1.	RBC (10^6/µl)	10.3 ± 2.2	9.9 ± 0.9	11.2 ± 0.43	9.58 ± 1.15	12.18 ± 0.91	6.93-12.24
2.	HCT (%)	46.4 ± 1.5	43.91 ± 1.7	45.9 ± 1.34	46.43 ± 2.34	52.11± 1.49	42.1-68.3
3.	MCV (fL)	53.1 ± 1.9	54.5 ± 2.5	56.7 ± 0.43	61.92 ± 0.45	63.9 ± 1.4	50.7-64.4
4.	WBC (10^3/µl)	4.49 ± 1.2	5.32 ± 0.28	7.64 ± 1.59	7.35 ± 0.38	9.79 ± 2.25	3.48-14.03
5.	Neutrophils (%)	10.8 ± 1.4	15.9 ± 0.73	17.42 ± 1.9	16.29 ± 3.75	24.42 ± 1.6	9.8-39.11
6.	Lymphocytes (%)	54.8 ± 0.5	55.91 ± 0.3	63.24± 2.8	64.35 ± 2.1	72.33 ± 2.81	48.81-83.19
7.	Monocytes (%)	6.34 ± 0.3	9.34 ± 0.95	7.38 ± 1.12	5.59 ± 2.39	9.42 ± 1.45	3.29-12.48
8.	Eosinophils (%)	0.4 ± 0.23	0.5 ± 0.11	2.3 ± 0.91	3.42 ± 0.52	4.15 ± 0.34	0-4.9

9.	Basophils (%)	0.2 ± 0.15	0.95 ± 0.7 1.4 ± 0.11	1.39 ± 0.34 1.45 ± 0.21	0-1.8
10.	Platelets (10^3/µl)	91 ± 5.8	434 ± 13.4 632 ± 11.3	579 ± 14.38 714 ± 9.36	420-1698
11.	Glucose (mg/dl)	169 ± 7.1	174 ± 3.49 195 ± 2.54	159 ± 9.42 178 ± 7.68	129-329
12.	Creatinine (mg/dl)	0.41 ± 0.003	0.49 ± 0.01 0.39 ± 0.06	0.26 ± 0.07 0.38 ± 0.12	0.2-0.4
13.	Total Bilirubin (mg/dl)	0.3 ± 0.001	0.4 ± 0.04 0.36 ± 0.02	0.42 ± 0.02 0.46 ± 0.06	0.2-0.5
14.	ALT (U/I)	59.4 ± 3.1	69.8 ± 4.4 78.32 ± 15.1	75.49 ± 7.45 97.36 ± 4.39	41-131
15.	AST (U/I)	65 ± 10.9	74.5 ± 5.21 83.98 ± 3.4	79.21 ± 6.94 95.91± 2.91	55-352
16.	ALP (U/I)	221 ± 12.9	215.7 ± 14.3 239 ± 22.6	229.9 ± 17.3 245.3 ± 11.2	118-433

Table 4: Effect of **(1)** and **(2)** on biochemical and haematological parameters in Female BALB/c mice. Values are expressed as mean ± SEM for five female mice in each group. RBC: red blood count; HCT: hematocrit; MCV: mean corpuscular volume; WBC: white blood cells; ALT: alanine aminotransferase; AST: aspartate aminotransferase; ALP: alkaline phosphatase.

4.13. Tissue collection and histopathological analysis

Microscopic evaluation of animals in both experimental and control groups showed no pathological alteration. In the test groups of animals, no toxic or toxico-allergic effects of **(1)** and **(2)** were found. Various parts of the kidney, including renal corpuscles, tubules, blood vessels, and interstitium in the cortex, medulla, and papilla, were examined, and there was no evidence of pathological effects. Also, microscopic examination of different liver parts showed no significant pathological changes. In the microscopic evaluation of the lungs, all the muscular layers and air sacs were examined, and there is no evidence of pathological effects (Figure 12).

Kidney:

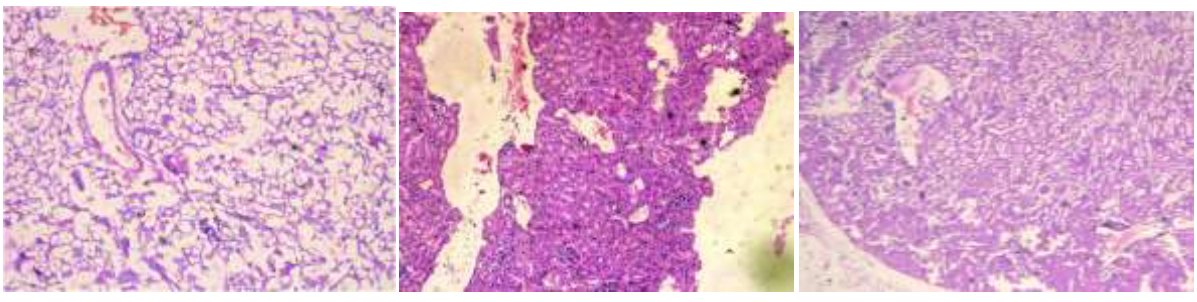

Control LPS Dexa

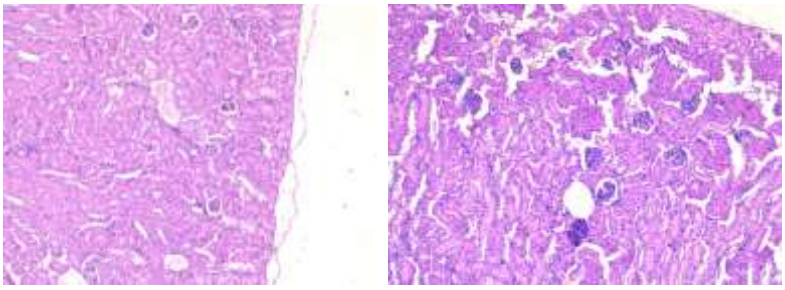

(1) **(2)**

Liver:

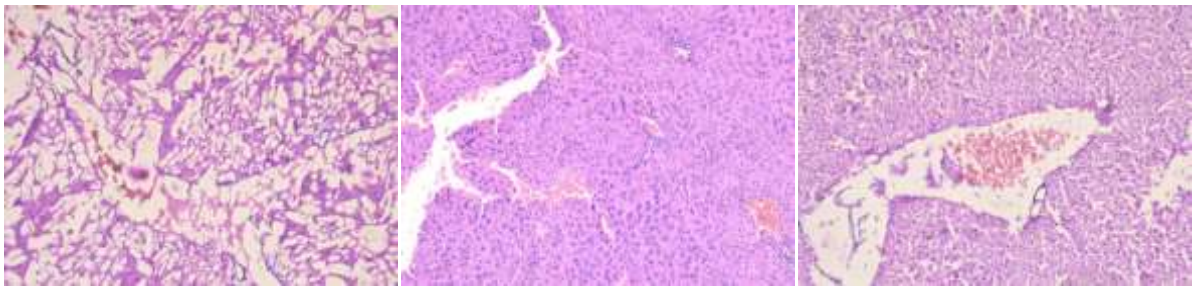

Control LPS Dexa

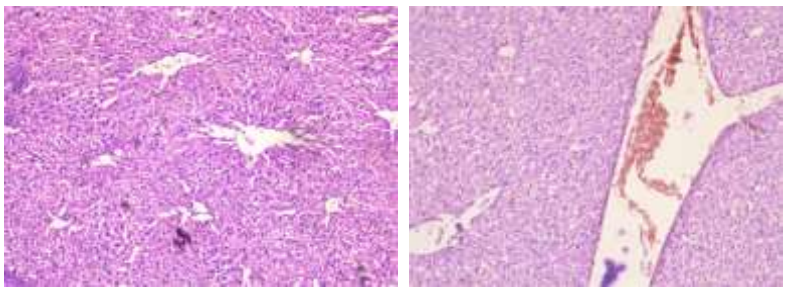

(1) **(2)**

Lungs:

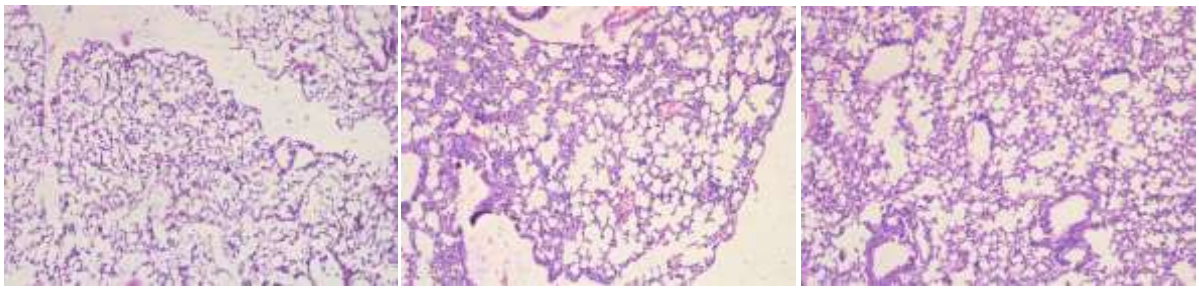

Control LPS Dexa

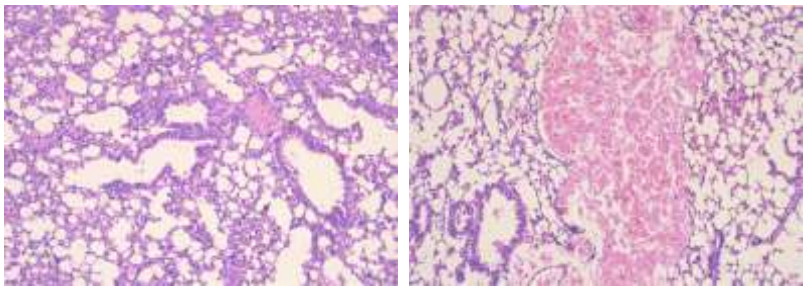

(1) **(2)**

Figure 12: Histopathological analysis of kidney, liver, and lung tissues. **(2)** (40 mg/kg) protects the liver, kidney, and lungs from damage more than its parent compound, **(1)** (40 mg/kg). BALB/c mice were injected with **(1)** and **(2)** (40 mg/kg), 1hr before LPS injection (1

mg/kg i.p), and kidney, liver, and lungs tissues were harvested 24hrs after LPS injection. These results depict H&E staining of a liver tissue section from the indicated group (40x magnification).

Discussion

The majority of therapeutics that have been discovered has been built on the structural diversity of natural compounds, which frequently interact with a wide range of biological targets. These compounds can either be found in their whole or as semi-synthetic derivatives. The most often prescribed medications in clinical and veterinary settings for the management of inflammatory disorders globally are NSAIDs [31]. Despite the medication's undeniable clinical efficacy, there is a substantial risk of adverse responses, including myocardial infarction, cardiac sudden death, liver and kidney damage, allergic reactions, gastrointestinal bleeding or ulcers, and allergic reactions. 25 % of patients typically have adverse effects, and 5 percent of those cases result in imminent death. Dexamethasone and Diclofenac are the most potent NSAIDs, and long-term use of the medication can cause serious pathologic side effects including cardiovascular issues, peptic ulcers, hepatotoxicity, gastrointestinal bleeding, renal papillary necrosis, and renal failure [32]. This necessitates the quest for stronger and safer analgesic and anti-inflammatory drugs.

The primary objective of the present study was to investigate the anti-inflammatory potential of the synthesised derivative, **(2)** as compared to its parent molecule, Arteannuin-B **(1)**. The compound library consisting of ~15 compounds were screened by using different methods and ~05 hits were obtained. In our previous study, we found that the synthetic derivatives of **(1)** strongly inhibit TNF-α and IL-6 in a dose dependent manner. Therefore, we continued the *in-vitro* research on the possible inhibitory impact on pro-inflammatory mediators in LPS-stimulated RAW 264.7 and *in-vivo* female BALB/c mice for validation. Without changing cell survival or shape, **(2)** significantly reduced the inflammatory responses in LPS-stimulated macrophages. In our experimental design, treatment with **(2)** significantly outperformed regular dexa in terms of its ability to suppress NO generation induced by LPS with an effectiveness equivalent to that of its parent molecule. Several studies have demonstrated that LPS induces NF-κB/IκBα pathway resulting in the stimulation of production of pro-inflammatory cytokines and chemokines. An appealing target for anti-inflammatory treatments has shown to be NF-κB, a transcription factor that is redox sensitive [33]. Its activation is strictly regulated by the phosphorylation of IkB caused by the inhibitor of NF-kB (IκB) kinase (IKK), which at rest sequesters NF-κB in the cytoplasm. NF-κB is free to go into the nucleus when IκB is destroyed by IKK-mediated phosphorylation, where it attaches to the promoters of genes containing κB sites, such as iNOS [34].

Our study demonstrated that **(2)** has the capacity to suppress the LPS-induced degradation of IκBα as well as NF-κB p65 nuclear translocation. These western blotting results unequivocally showed that **(2)** effectively inhibits LPS-induced NF-κB activation to control the production of iNOS. In addition to regulating the expression of cytokines like TNF-α and IL-6, NF-κB is essential for the development of pro-inflammatory enzymes. ELISA results also confirmed the inhibitory effect of **(1)** and **(2)** in the production of TNF-α and IL-6. An

excessive quantity of ROS is released by activated macrophages during inflammation [35], and flow cytometric measurement of intracellular ROS levels in LPS-stimulated RAW 264.7 cells showed that pretreatment with **(2)** greatly reduced the excessive ROS production caused by LPS. To extend these results, we investigated the *in-vivo* efficacy of the drug molecules to understand the therapeutic potential. Bioinformatic analysis was also performed so as to find out the target docking site and to find out the cys score. Additionally, light microscopy study showed no adverse effects of the **(1)** and **(2)** concentrations employed in animals; nevertheless, mice treated with carrageenan showed buildup of infiltrating inflammatory cells, vascular congestion, and a severe necrotic response. Additionally, the biochemical toxicity indicators did not exhibit any abnormalities.

The primary issue brought on by inflammation is pain, which should be reduced by an anti-inflammatory drug (analgesic action), either directly by targeting the pain receptors or indirectly by lowering edema and erythema [36]. **(2)** has shown an increase in reaction time in response to thermally produced pain when tested for the analgesic/anti-nociceptive activity utilizing the tail immersion test. In addition, the outcomes of the carrageenan induced odema experiment and the acetic acid-induced writhing assay demonstrated the potency of **(2)** against chemically generated pain.

(2) being a potent anti-inflammatory and analgesic semi-synthetic compound, with a wide safety window, showed almost higher efficacy over the most popular NSAIDs. Even **(2)** is being administered at a low dose of 1mg/kg indicating its therapeutic potential to be in the drug pipeline. Therefore **(2)** can be a suitable candidate for further exploration of its potential against diseased models for chronic-inflammatory conditions and detailed mechanistic studies for the underlying mechanism of action.

Conclusion

In conclusion, we discovered that as compared to **(1)**, **(2)** effectively inhibited LPS-stimulated macrophage inflammatory responses and also proved to be anti-analgesic for the treatment of inflammation. As a result, our research leads us to believe that the natural component derivative **(2)** may be a cutting-edge anti-inflammatory drug.

Authors contribution GS: Investigation, Methodology, Writing-original draft, conceptualisation. JR: Investigation and synthesis of drug molecules. DS: Formal Analysis. MO: Planning of experiments. SP: Conceptualization, Investigation and review. FB: Investigation. BA: Formal analysis. AB: Investigation. AA: Investigation. ZA: Validation, Supervision, Project administration, Funding acquisition.

All authors read and approved the manuscript and all data were generated in-house and that no paper mill was used.

Funding source Not Applicable.

Data availability All data generated or analyzed during this study are included in this article (and its supplementary information files).

Declarations

Ethical approval All animal studies followed the guidelines laid out in the Guide for the Care and Use of Laboratory Animals (National Research Council 2011). The Institutional Animal Ethics Committee (180/75/8/2019) authorized all of the protocols employed in the experiment.

Consent to participate Not Applicable.

Consent to publish Not Applicable.

Competing interests The authors declare that they have no competing interest.

Acknowledgment The authors would like to express their utmost gratitude and appreciation to the Director, CSIR-Indian Institute of Integrative Medicine and Department of Science and Technology- India for providing a research fellowship to Gifty Sawhney via fellowship code no. DST/INSPIRE Fellowship/2017/IF170212. We also thank International Centre for Genetic Engineering and Biotechnology for providing Arturo-Falaschi Short-term PhD Fellowship (F/IND19-11) at ICGEB-Cape Town.

Abbreviations

%: Percentage
ALT: Alanine aminotransferase
AST: Aspartate aminotransferase
ALP: Alkaline phosphatase
Dexa: Dexamethasone
DCFH-DA: Dichloro-dihydro-fluorescein diacetate
HCT: Hematocrit
iNOS: Inducible nitric oxide synthase
IL-6: Interleukin-6
LPS: Lipopolysaccharide
MCV: Mean corpuscular volume
NF-κB: Nuclear factor-kappa B
NO: Nitric oxide
RBC: Red blood count
ROS: Reactive oxygen species
TNF-α: Tumor necrosis factor-alpha
WBC: White blood cells

Supplementary information:

The document related to the supplementary information has been uploaded in the portal.

References

1. Medzhitov, R., *Origin and physiological roles of inflammation.* Nature, 2008. **454**(7203): p. 428-435.

2. Serhan, C.N., *Resolution phase of inflammation: novel endogenous anti-inflammatory and proresolving lipid mediators and pathways.* Annu. Rev. Immunol., 2007. **25**: p. 101-137.
3. Schett, G., *Rheumatoid arthritis: inflammation and bone loss.* Wiener Medizinische Wochenschrift, 2006. **156**(1): p. 34-41.
4. Karin, M. and F.R. Greten, *NF-κB: linking inflammation and immunity to cancer development and progression.* Nature reviews immunology, 2005. **5**(10): p. 749-759.
5. Libby, P., P.M. Ridker, and A. Maseri, *Inflammation and atherosclerosis.* Circulation, 2002. **105**(9): p. 1135-1143.
6. Hiraiwa, K. and S.F. van Eeden, *Contribution of lung macrophages to the inflammatory responses induced by exposure to air pollutants.* Mediators of inflammation, 2013. **2013**.
7. Chakraborty, P., G. Saraswat, and S.N. Kabir, *α-Dihydroxychalcone-glycoside (α-DHC) isolated from the heartwood of Pterocarpus marsupium inhibits LPS induced MAPK activation and up regulates HO-1 expression in murine RAW 264.7 macrophage.* Toxicology and applied pharmacology, 2014. **277**(1): p. 95-107.
8. Fujiwara, N. and K. Kobayashi, *Macrophages in inflammation.* Current Drug Targets-Inflammation & Allergy, 2005. **4**(3): p. 281-286.
9. Dinkova-Kostova, A., et al., *Phenolic Michael reaction acceptors: combined direct and indirect antioxidant defenses against electrophiles and oxidants.* Medicinal Chemistry, 2007. **3**(3): p. 261-268.
10. Patel, S.A., et al., *Inflammatory mediators: parallels between cancer biology and stem cell therapy.* Journal of inflammation research, 2009. **2**: p. 13.
11. Lee, C.W., et al., *Hederagenin, a major component of Clematis mandshurica Ruprecht root, attenuates inflammatory responses in RAW 264.7 cells and in mice.* International immunopharmacology, 2015. **29**(2): p. 528-537.
12. Ghosh, S. and M. Karin, *Missing pieces in the NF-κB puzzle.* cell, 2002. **109**(2): p. S81-S96.
13. Li, Q. and I.M. Verma, *NF-κB regulation in the immune system.* Nature reviews immunology, 2002. **2**(10): p. 725-734.
14. Novotny, N.M., et al., *Differential IL-6 and VEGF secretion in adult and neonatal mesenchymal stem cells: role of NFkB.* Cytokine, 2008. **43**(2): p. 215-219.
15. Dinarello, C.A., *Anti-inflammatory agents: present and future.* cell, 2010. **140**(6): p. 935-950.
16. Sören, B. and C. Steven, *Functions of NF-κB1 and NF-κB2 in immune cell biology.* Biochem J, 2004. **382**: p. 393-409.
17. Hernández-Guerrero, C.J., et al., *Cytotoxic dibromotyrosine-derived metabolites from the sponge Aplysina gerardogreeni.* Bioorganic & medicinal chemistry, 2007. **15**(15): p. 5275-5282.
18. Hidalgo, M., et al., *A Phase I and pharmacological study of the glutamine antagonist acivicin with the amino acid solution aminosyn in patients with advanced solid malignancies.* Clinical cancer research, 1998. **4**(11): p. 2763-2770.
19. Bohac, T.J., J.A. Shapiro, and T.A. Wencewicz, *Rigid oxazole acinetobactin analog blocks siderophore cycling in Acinetobacter Baumannii.* ACS infectious diseases, 2017. **3**(11): p. 802-806.
20. Ichiba, T., P.J. Scheuer, and M. Kelly-Borges, *Three bromotyrosine derivatives, one terminating in an unprecedented diketocyclopentenylidene enamine.* The Journal of Organic Chemistry, 1993. **58**(15): p. 4149-4150.
21. Shaala, L.A., et al., *Subereamolline A as a potent breast cancer migration, invasion and proliferation inhibitor and bioactive dibrominated alkaloids from the Red Sea sponge Pseudoceratina arabica.* Marine drugs, 2012. **10**(11): p. 2492-2508.
22. von Nickisch-Rosenegk, E., D. Schneider, and M. Wink, *Carrier-Mediated Uptake of Cardenolides and of Quinolizidine Alkaloids by Larvae of Syntomeida epilais and Uresiphita reversalis.* Planta Medica, 1990. **56**(06): p. 624-625.

23. Hoffstrom, B.G., et al., *Inhibitors of protein disulfide isomerase suppress apoptosis induced by misfolded proteins.* Nature chemical biology, 2010. **6**(12): p. 900-906.
24. Li, Y., *Qinghaosu (artemisinin): chemistry and pharmacology.* Acta Pharmacologica Sinica, 2012. **33**(9): p. 1141-1146.
25. Lee, S.K., et al., *Artemisia annua extract prevents ovariectomy-induced bone loss by blocking receptor activator of nuclear factor kappa-B ligand-induced differentiation of osteoclasts.* Scientific reports, 2017. **7**(1): p. 1-12.
26. Rasool, J.U., et al., *Site Selective Synthesis and Anti-inflammatory Evaluation of Spiro-isoxazoline Stitched Adducts of Arteannuin B.* Bioorganic Chemistry, 2021: p. 105408.
27. Cao, Y. and L. Li, *Improved protein–ligand binding affinity prediction by using a curvature-dependent surface-area model.* Bioinformatics, 2014. **30**(12): p. 1674-1680.
28. Daina, A., O. Michielin, and V. Zoete, *SwissADME: a free web tool to evaluate pharmacokinetics, drug-likeness and medicinal chemistry friendliness of small molecules.* Scientific reports, 2017. **7**(1): p. 1-13.
29. Shi, J.Q., et al., *Antimalarial drug Artemisinin extenuates amyloidogenesis and neuroinflammation in APP swe/PS 1dE9 Transgenic Mice via inhibition of nuclear factor-κ B and NLRP 3 Inflammasome Activation.* CNS neuroscience & therapeutics, 2013. **19**(4): p. 262-268.
30. Robert, A., et al., *The antimalarial drug artemisinin alkylates heme in infected mice.* Proceedings of the National Academy of Sciences, 2005. **102**(38): p. 13676-13680.
31. Munford, R.S. and J. Pugin, *Normal responses to injury prevent systemic inflammation and can be immunosuppressive.* American journal of respiratory and critical care medicine, 2001. **163**(2): p. 316-321.
32. Aydin, G., et al., *Histopathologic changes in liver and renal tissues induced by different doses of diclofenac sodium in rats.* Turkish Journal of Veterinary & Animal Sciences, 2003. **27**(5): p. 1131-1140.
33. Medzhitov, R. and T. Horng, *Transcriptional control of the inflammatory response.* Nature reviews immunology, 2009. **9**(10): p. 692-703.
34. Liu, F., et al., *IKK biology.* Immunological reviews, 2012. **246**(1): p. 239-253.
35. Lee, Y., et al., *Src kinase-targeted anti-inflammatory activity of davallialactone from Inonotus xeranticus in lipopolysaccharide-activated RAW264. 7 cells.* British journal of pharmacology, 2008. **154**(4): p. 852-863.
36. Seoudi, D., et al., *Evaluation of the anti-inflammatory, analgesic, and anti-pyretic effects of Origanum majorana ethanolic extract in experimental animals.* Journal of Radiation Research and Applied Sciences, 2009. **2**(3): p. 513-534.

Supplementary Files

This is a list of supplementary files associated with this preprint. Click to download.

- Supplementarydata.docx
- Onlinefloatimage1.png